Investigation of the slow relaxation of the magnetization dynamics in homoleptic ene-diamido organodysprosium(iii) complexes with K + /arene interactions

Jérome Long, Aleksei Tolpygin, Anton Cherkasov, Konstantin A. Lyssenko, Yannick Guari, Joulia Larionova, Alexander Trifonov

Investigation of the Slow Relaxation of the Magnetization Dynamics in Homoleptic Ene-Diamido Organodysprosium(III) Complexes with K^+/Arene Interactions

Jérôme Long*,[a] Aleksei O. Tolpygin,[b] Anton V. Cherkasov,[b] Konstantin A. Lyssenko,[c,d] Yannick Guari,[a] Joulia Larionova,[a] Alexander A. Trifonov*[b,c]

We report the synthesis, structure and magnetic investigations of two new Dy^{3+} homoleptic ate-complexes based on different ene-diamido ligands $[K(THF)_2][Dy(DAD^{2R})2]$ (R = H (**1**), Me (**2**) DAD^{2R} = [2,6-$iPr_2C_6H_3N$–CR=CR–$NC_6H_3iPr_2$-2,6 showing K^+/Arene interactions. Magnetic investigations reval that both compounds exhibit a zero-field Single-Molecule Magnetic relaxation mainly governed by a Raman process.

Introduction

The ability of some mononuclear lanthanide complexes to exhibit slow relaxation of their magnetization possibly associated with magnetic bistability at the molecular scale opens exciting avenues for the information storage or spin-based computing.[1-4] In these so-called Single-Molecule Magnets (SMMs), the optimum balance between the specific 4*f* electronic density of defined lanthanide ions with the coordinated ligands engenders a crystal-field splitting which could lead to the appearance of an anisotropic barrier, Δ, separating opposite orientations ($\pm m_J$) of the magnetic moments.[5-8] It is generally recognized that in efficient genuine SMMs, the energy barrier should be as large as possible and the retention of the magnetization (with hysteresis effect) should be achieved in zero magnetic field below a blocking temperature, which should be the highest possible.[9] The theoretical modelling predicted, some years ago, that the most efficient strategy to fulfill such objectives consists in stabilizing the oblate electronic density of Dy^{3+} ion by an axial crystal-field generated by the presence of two negatively charged ligands along an axis with short bond lengths and no coordinated species in the equatorial plane.[5, 10] This targeted environment permits to maximize the crystal-field splitting when a suitable symmetry is achieved. Such approach has been nicely demonstrated in both, coordination complexes[11-18] and organometallic metallocene complexes[19-20] with magnetic hysteresis observed up to 80 K.[21] Yet, these studies point out that additional processes, such as the Quantum Tunnelling of the Magnetization (QTM), as well as Raman and direct relaxations, may greatly complicate the overall relaxation mechanism by creating underbarrier pathways, reducing the SMMs hallmarks.[22-23] For instance, the exceptional magnetic performances of dysprosium metallocene family could be ascribed, not only to the tailored coordination environment, but also to the reduced molecular vibrations (vibrational modes) imposed by the rigid cyclopentadienyl ligands.[20-21, 23-25] It appears therefore critical, with the aim to ultimately optimize the SMMs, to gain deeper insights on the parameters affecting such spin-phonon coupling.

Following this idea, we have recently investigated the use of diazabutadiene ligands for the design of lanthanide SMMs.[26-27] These doubly negatively charged ligands could act both, as *n* and π-electron donors, while benefiting from a great tunability with respect to their steric and electronic features. Hence, we have previously shown that an homoleptic $[Li(DME)_3][Dy(DAD^{2H})_2]$ complex (DAD^{2H} = [2,6-$iPr_2C_6H_3N$–CH=CH–$NC_6H_3iPr_2$-2,6], DME = dimethoxyethane) exhibit a genuine SMM behaviour with a significant axial crystal-field.[27] However, despite this noticeable crystal-field splitting generated by the DAD ligands, the Raman process was found to dominate the relaxation dynamics. In order to increase the rigidity of the system and circumvent such Raman relaxation, half-sandwich heteroleptic complexes $[Dy(DAD^{2Me})Cp^*Cl]$ and $[Li(THF)_3][Dy(DAD^{2Me})Cp^*Cl]$ (DAD^{2Me} = [2,6-$iPr_2C_6H_3N$–CMe=CMe–$NC_6H_3iPr_2$-2,6], Cp^* = C_5Me_5) were also designed by associating DAD-type ligands providing short Dy-N distances with a rigid Cp* moiety.[28] However, in the previous examples, an additional ligand (Cl or THF) was coordinated in the equatorial plane that in turn decreases the axiality. Encouraged by these results, we continued to explore the potential of the DAD ligands. We report here, the synthesis, structure and magnetic investigations of two cationic homoleptic complexes of Dy^{3+} based on distinct dianionic DAD ligands with unusual K^+/arene interactions and exhibiting a zero-field SMM behaviour. Remarkably, although the nature of the substituent on the DAD ligand and counter-ion directly affects the Dy^{3+} coordination sphere, the magnetization is found to relax mainlt *via* a Raman process.

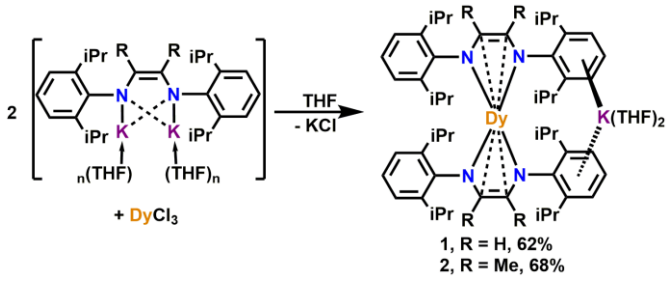

Scheme 1. Synthesis of complexes **1** and **2**.

Experimental

Materials and Methods

General Procedures

All operations were carried out under an atmosphere of argon using Schlenk techniques or in a nitrogen filled glovebox. THF and toluene were purified by distillation from sodium/benzophenone ketyl and degassed thoroughly. Hexane was dried by distillation from sodium/triglyme and benzophenone ketyl prior to use. $DyCl_3$,[29] and DAD[2R] (2,6-*i*PrC_6H_3-NC(R)C(R)NC_6H_3*i*Pr-2,6)[30] (R = H, Me) were prepared according to literature procedures. Lanthanide metal analysis was carried out by complexometric titration.[31] IR spectra were recorded as Nujol mulls on a Bruker-Vertex 70 spectrophotometer. Elemental analysis was performed in the microanalytical laboratory of IOMC.

Synthesis of [K(THF)$_2$][Dy(2,6-*i*Pr$_2$C$_6$H$_3$NCHCHNC$_6$H$_3$*i*Pr$_2$-2,6)$_2$] (1).

A solution of $K_2(THF)_n$[2,6-*i*Pr$_2$$C_6H_3$NCHCHN$C_6H_3$*i*Pr$_2$-2,6] *in situ* prepared from 2,6-*i*Pr$_2$$C_6H_3$NCHCHN$C_6H_3$*i*Pr$_2$-2,6 (0.75 g, 1.99 mmol) and K shavings (0.16 g, 3.98 mmol) in 30 mL of THF was slowly added to a suspension of $DyCl_3$ (0.27 g, 0.99 mmol) in 5 mL of THF. The reaction mixture was stirred for 12 h at ambient temperature. The volatiles were removed in vacuum and the solid residue was extracted with toluene (40 mL). The toluene extract was filtered, toluene was removed in vacuum. Recrystallization of the resulting solid from THF/hexane mixture at 20 °C afforded orange crystals of **1** (0.68 g, 0.62 mmol, 62% yield). Elemental analysis calcd. (%) for $C_{60}H_{88}DyKN_4O_2$ (1098.96g·mol^{-1}): C, 65.57; H, 8.07; Dy, 14.79; N, 5.10; found (%): C, 65.78; H, 7.93; Dy, 14.90; N, 5.21. IR (Nujol, KBr) v/cm^{-1}: 1919 (w), 1855 (w), 1836 (w), 1794 (w), 1628 (s), 1581 (s), 1563 (m), 1530 (s), 1429 (s), 1368 (s), 1334 (s), 1309 (s), 1265 (s), 1224 (s), 1208 (s), 1178 (s), 1151 (m), 1141 (m), 1107 (s), 1074 (s), 1050 (s), 1005 (s), 922 (s), 890 (s), 871 (s), 819 (s), 796 (s), 770 (s), 760 (s), 744 (s).

Synthesis of [K(THF)$_2$][Dy(2,6-*i*Pr$_2$C$_6$H3NCMeCMeNC$_6$H$_3$iPr2-2,6)$_2$] (2).

A solution of $K_2(THF)_n$[2,6-*i*Pr$_2$$C_6H_3$NCMeCMeN$C_6H_3$*i*Pr$_2$-2,6] *in situ* prepared from 2,6-*i*Pr$_2$$C_6H_3$NCMeCMeN$C_6H_3$*i*Pr$_2$-2,6 (0.80 g, 1.98 mmol) and K shavings (0.15 g, 3.95 mmol) in 30 mL of THF was slowly added to a suspension of $DyCl_3$ (0.27 g, 0.99 mmol) in THF (5 mL) at room temperature. The reaction mixture was stirred for 12 h at ambient temperature. The volatiles were evaporated and the solid residue was extracted with toluene (40 mL). The toluene extract was filtered, toluene was removed in vacuum. Recrystallization of the resulting solid from THF/hexane mixture at 20 °C afforded orange crystals of **2** (0.78 g, 0.67 mmol, 68% yield). Elemental analysis calcd. (%) for $C_{64}H_{96}DyKN_4O_2$ (1155.07g·mol^{-1}): C, 66.55; H, 8.38; Dy, 14.07; N, 4.85; found (%): C, 66.81; H, 8.11; Dy, 14.00; N, 4.69. IR (Nujol, KBr) v/cm^{-1}: 1914 (w), 1882 (w), 1835 (w), 1786 (w), 1645 (s), 1583 (s), 1560 (m), 1425 (s), 1362 (s), 1337 (s), 1254 (s), 1204 (s), 1156 (c), 1138 (s), 1111 (s), 1049 (s), 936 (s), 887 (s), 863 (s), 818 (s), 799 (m), 789 (m), 775 (s), 758 (s), 744 (s).

X-Ray crystallography

The X-ray data for **1** and **2** were collected with *Bruker Smart Apex II* (**1**) and *Rigaku OD Xcalibur* (**2**) diffractometers ($Mo_{K\alpha}$-radiation, ω-scans technique, λ = 0.71073 Å) using *APEX3*[32] and *CrysAlis Pro* [33] software packages. The structures were solved by direct methods and were refined by full-matrix least squares on F^2 for all data using *SHELX*.[34] *SADABS*[35] and *SCALE3 ABSPACK* scaling algorithm implemented in *CrysAlis Pro* were used to perform absorption corrections. All non-hydrogen atoms in **1** and **2** and hydrogen atoms of NCCN fragments in **1** were found from Fourier syntheses of electron density (all non-hydrogen atoms were refined anisotropically). All other hydrogen atoms were placed in calculated positions and were refined in the "riding" model with $U(H)_{iso} = 1.2U_{eq}$ of their parent atoms ($U(H)_{iso} = 1.5U_{eq}$ for methyl groups). Disordered fragments in both structures were restrained using *AFIX*, *DFIX*, *SADI* and *FLAT* instructions. Displacement parameters of non-hydrogen atoms of disordered fragments in **1** and all non-hydrogen atoms in **2** were restrained using *RIGU* instruction.
The crystallographic data and structures refinement details are given in Table S1. CCDC–1994537 (**1**) and 1994538 (**2**) contains the supplementary crystallographic data for this paper. These data are provided free of charge by The Cambridge Crystallographic Data Centre: ccdc.cam.ac.uk/structures. The corresponding CIF files are also available in the Supporting Information.

Magnetic Measurements

Magnetic susceptibility data were collected with a Quantum Design MPMS-XL SQUID magnetometer working in the range 1.8–300 K with the magnetic field up to 7 Tesla. The samples were prepared in a glove box. The data were corrected for the sample holder and the diamagnetic contributions calculated from the Pascal's constants. The AC magnetic susceptibility measurements were carried out in the presence of a 3 Oe oscillating field in zero or applied external DC field.

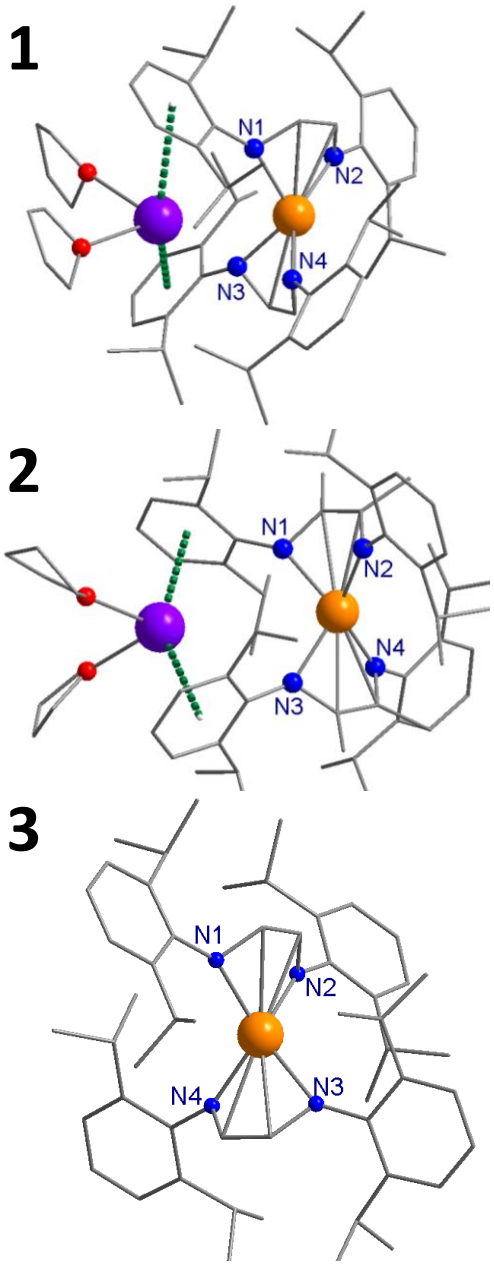

Fig. 1. Molecular structure of **1** and **2** and **3**.[27] Color code: orange, Dy; red, O; grey, C; purple, K. Hydrogen atoms and Li^+ ion (for **3**) have been omitted for clarity.

Results and Discussions

Synthesis and crystal structures

The synthetic strategy to design the targeted homoleptic ate-complexes relies on the salt metathesis reactions of anhydrous $DyCl_3$ with two-fold amounts of $[K(THF)_n][DAD^{2R}]$ (R = H, Me), *in situ* prepared from DAD^{2R} and potassium shavings and giving $[K(THF)_2][Dy(DAD^{2R})_2]$ (X = H (**1**), Me (**2**)) (Scheme 1). The reactions were carried out at 25 °C in THF solution within 24 h. After recrystallization from a THF/hexane mixture, complexes **1** and **2** were isolated as orange crystals in 62 and 68% yields, respectively.

Table 1: Some structural parameters for compounds **1-3.**

Compound	Dy-N distances / Å	DAD-DyDAD Angle NCCN centroids / °	Trans N-Dy-N angles	Ref.
1	2.239(2) 2.248(2) 2.266(2) 2.268(2)	164.5	109.34(5) 152.85(5)	This work
2	2.231(2) 2.238(2) 2.248(2) 2.259(2)	177.5	126.39(6) 128.78(6)	This work
3	2.221(3) 2.226(4) 2.246(3) 2.256(3)	172.2	125.01(7) 138.27(7)	27

The X-ray diffraction study revealed that the homoleptic complexes crystallize in the triclinic $P\bar{1}$ (**1**) and monoclinic $P2_1/n$ (**2**) space groups, respectively, with one molecule of ate-complex in the asymmetric unit (Fig. 1, Table S1). The Dy^{3+} cation presents a comparable lanthanide coordination environment, reminiscent to the recently described $[Li(DME)_3][Dy(DAD^{2H})_2]$ (**3**) complex.[27] It simply consists of two $2\sigma{:}\eta^2$-coordinated dianionic DAD ligands, the overall negative charge being compensated by a coordinated potassium ion in proximity with the Dy^{3+}, the shortest Dy^{3+}-K^+ distances being equal to 3.6548(8) and 4.6851(7) Å for **1** and **2**, respectively. The K^+ cation interacts with one phenyl ring of each DAD ligand and completes its coordination sphere with two THF molecules. It is worthy of note that the two K···Ar_{centre} (Ar for aryl substituent of DAD) distances in **1** are equal to 3.5071(9) and 4.0800(9) Å) and are much longer compared to those found in **2** (2.978(8) and 3.26(2) Å). Accordingly, different types of coordination of aryl substituents to potassium ion are observed in these complexes. Thus in **1**, the K^+ is η^2-coordinated by one aryl fragment resulting in short K···C distances of 3.071(2), 3.135(2) Å, while only one K···C short contact (3.249(2) Å) is observed for the second phenyl ring (K···C distances > 3.5 Å are declared as not bonding).[36-37] In **2**, the potassium ion is η^4-coordinated by one aryl fragment (3.175(2)-3.445(2) Å), whereas the interaction with the second one can be classified rather as η^6 (K···C: 3.175(2)-3.450(2) Å).

The Dy-N distances are in the ranges 2.239(2)-2.268(2) Å in **1** and 2.231(2)-2.259(2) Å in **2** (Table 1). Additionally, the presence of short Dy-C contacts (**1**: 2.622(2)-2.671(2) Å; **2**: 2.675(2)-2.699(2) Å) is indicative of η^2-coordination of C=C bond to Dy^{3+}. The Dy-N distances in **1** and **2** are slightly longer than those measured in the lithium analogue **3** (shortest distance is 2.221(3) Å, Table 1). The nature of the substituents by the imino carbons in the NCCN fragment affects the angle defined by the Dy^{3+} ion and the NCCN centroids of each DAD ligands ranging from 164.5 (complex **1**) to 177.5° (complex **2**) (Table 1). The shortest intermolecular Dy-Dy distances found by the analysis of the crystal packing (Fig. S1) are equal to 10.196(7) and 10.947(7) Å for **1** and **2**, respectively, indicating that the complexes are relatively well isolated.

Magnetic Properties

The magnetic properties were investigated in both, static and dynamic modes by using a SQUID MPMS-XL. The room temperature χT values of 13.12, and 13.42 $cm^3.K.mol^{-1}$ for **1** and **2**, respectively, are slightly lower than the value of 14.17 $cm^3.K.mol^{-1}$, expected for a unique Dy^{3+} ion using the free-ion approximation (Fig. 2). These lower experimental χT values may be rationalized by a significant crystal-field splitting.[6]

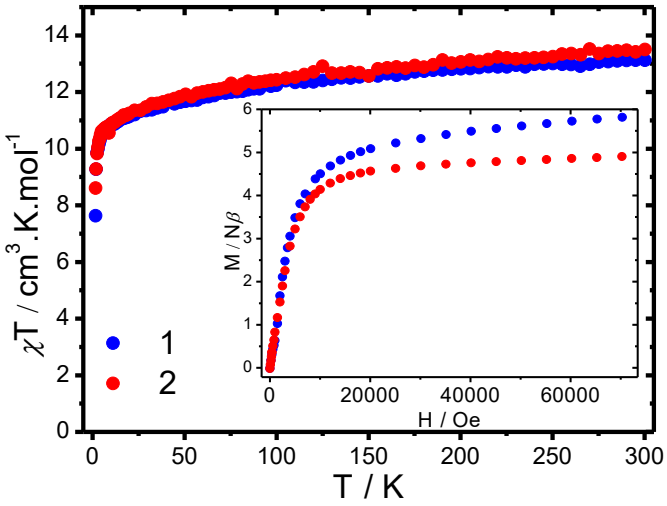

Fig. 2: Temperature dependence of χT under an applied magnetic field of 1000 Oe for **1** and **2**. Inset: field dependence of the magnetization at 1.8 K for **1** and **2**.

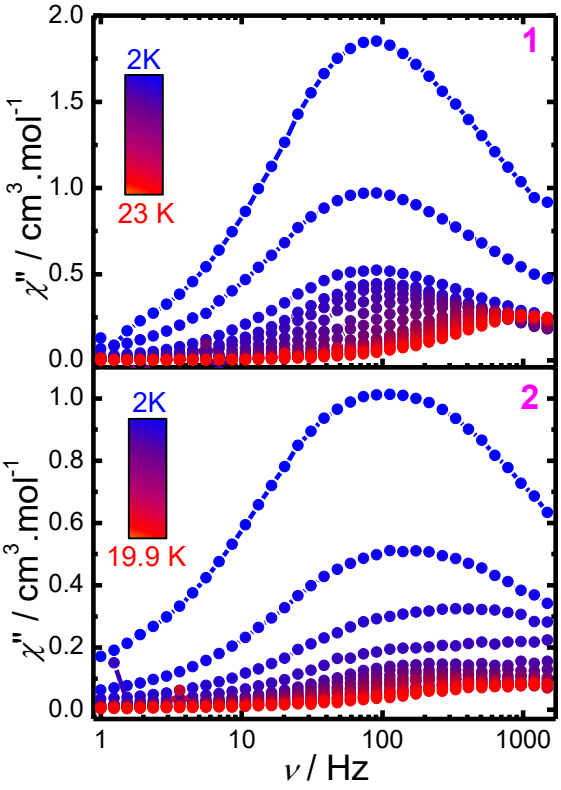

Fig. 3. Frequency dependence of the out-of-phase susceptibility component, χ'', for **1** and **2** under a zero dc-field.

Upon cooling, both samples exhibit a similar decrease of χT due to the thermal depopulation of the Stark sub-levels, while the field dependence of the magnetization at 1.8 K reveals the typical unsaturated curves with the values of 5.81 and 4.90 $N\beta$ under 70 kOe for **1** and **2**, respectively (Fig. 2). A clear opening in the hysteresis loops could be observed at low temperature for both compounds (Fig. S2), suggesting the occurrence of a slow relaxation of the magnetization.

This was further confirmed by using alternate currents (ac) measurements to study the relaxation dynamics. Both samples exhibit a clear frequency dependence of the in-phase (χ') and out-of-phase (χ'') components of the magnetic susceptibility (Fig. 3, Fig. S3-S4) indicating a SMM behavior. While for **1**, a single frequency dependent peak could be observed, **2** exhibits a broad peak at low temperature with the appearance of a plateau at high frequency upon increasing temperatures. Noticeably, such broad signals of χ'' have also been observed in heteroleptic dysprosium DAD^{2Me}/Cp* complexes with the same DAD^{2Me} ligand.[28] The corresponding Cole-Cole plots for **1** and **2** (Fig. 4) could be fitted with a generalized Debye model (Tables S2-S3), but this treatment gives large values for the α parameter, especially for **2** (about 0.4) indicating a large distribution of the relaxation times.[38] This could result in large uncertainties in the determination of the relaxation time, τ. Consequently, the program *CC-FIT2,* recently developed by *Reta and Chilton*,[39] was utilized to extract the τ values and the corresponding uncertainties from the underlying distribution function.

The τ *vs.* T plot (Fig. 5, Fig. S5) reveals a clear deviation at low temperatures, indicating the presence of several relaxation processes. It could be noticed that for **2**, the large values of the α parameter leads to important uncertainties for τ. For the three investigated compounds, the fitting was performed by considering the following equation: $\tau^{-1} = \tau_0^{-1}\exp(-\Delta/kT) + CT^n + \tau^{-1}_{QTM}$ (Eq. 1),[40] for which the first term accounts for a thermally activated process, while the second and third ones stand for two-phonon Raman and QTM, respectively. This however leads to small Δ barriers and/or large uncertainties (Table S4), suggesting that, as previously observed for **3**, the thermally activated Orbach process is not dominant or even not involved in the relaxation.[27] Consequently, the temperature dependence of the relaxation time was fitted with only a combination of Raman and QTM: $\tau^{-1} = CT^n + \tau^{-1}_{QTM}$ (Eq. 2). The best fit parameters could be found in Table 2. Despite the nice apparent fittings for all compounds (Fig. 5), the large uncertainties on the fit parameters obtained from the *CC-FIT2* software suggest that such analysis could only be considered as qualitative. For comparison, the fitting parameters by considering solely the extracted τ values (without taking into account the distribution of relaxation times) could be found in Table S5.

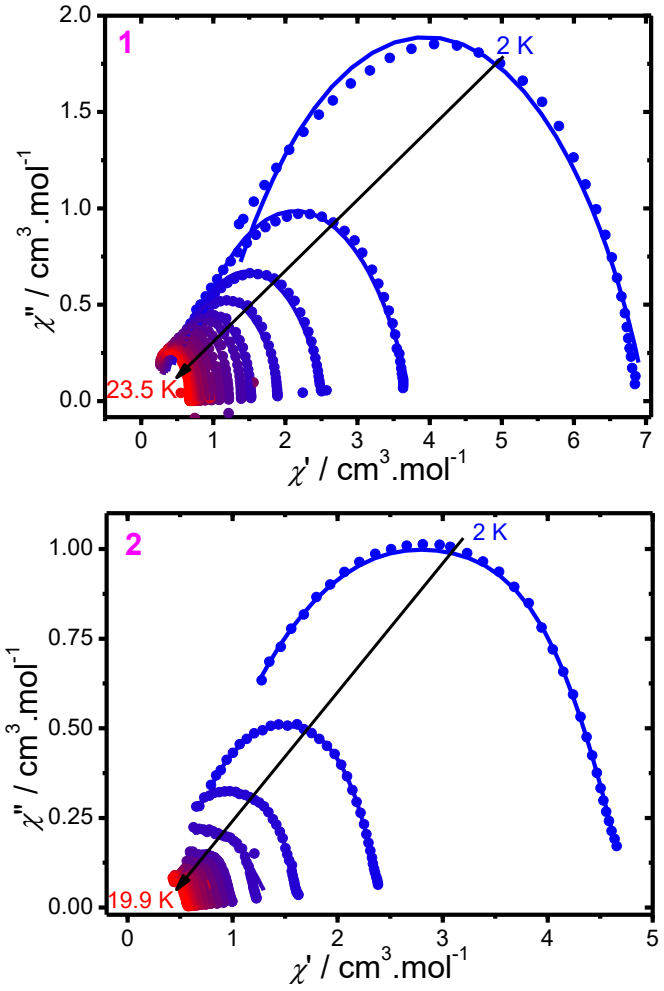

Fig. 4. Cole-Cole (Argand) plots obtained using the ac susceptibility data for **1** and **2** (0 Oe). The solid lines correspond to the best fit obtained with a Debye model.

For all compounds, the relaxation time becomes temperature independent at low temperature pointing out a significant QTM that could be shortcut by applying a dc magnetic field. Thus, the field dependence of the ac susceptibilities was monitored (Fig. S6, for **3** please refer to ref.[27]). For **2**, a second relaxation process could be discerned at high frequency upon applying dc fields but without a maximum.

Table 2: Fit parameters of the temperature dependence of the relaxation time for **1** and **2**.

Compound	*n*	C ($s^{-1}.K^{-m}$)	τ_{QTM} (s)
1 (0 Oe)	5(2)	$10^{-3(3)}$	$10^{-2.8(3)}$
1 (1000 Oe)	4.8(3)	$10^{-3.0(4)}$	-
2 (0 Oe)	4(7)	$10^{-1(9)}$	$10^{-3.1(5)}$
3 (0 Oe)	4(2)	$10^{-1(2)}$	$10^{-2.9(2)}$
3 (3500 Oe)	4.8(7)	$10^{-2.9(8)}$	-

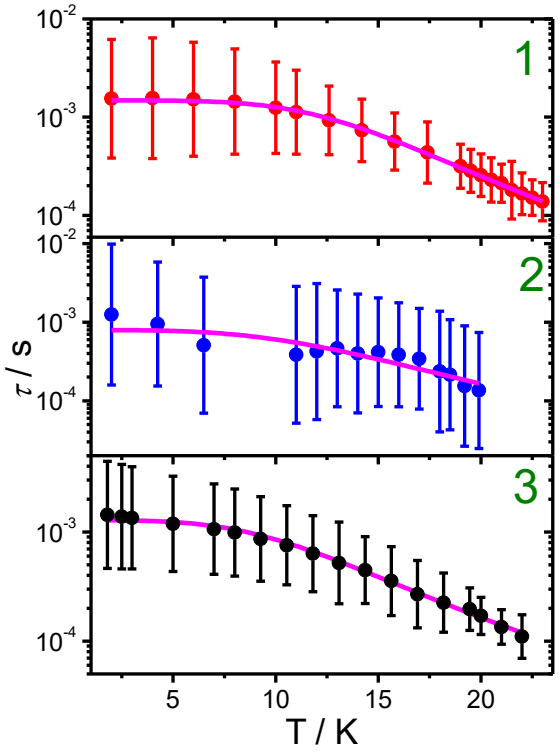

Fig. 5. Temperature dependence of the relaxation time, τ, for **1**-**3**. The uncertainties were determined from the CC-FIT2 software[39] while the solid magenta lines correspond to the fit with Eq. 2.

The corresponding field dependences of the relaxation time can be modelled with the equation, $\tau^{-1} = DH^4T + B_1/(1+B_2H^2) + K$ (Eq. 3), for which the first term accounts for the direct process (for Kramers-ion), the second one for the QTM, while the K constant accounts for Raman and thermally activated processes (Fig. S7, Table S6). The optimum field for which the relaxation time is the greatest is estimated at 1000 Oe and 2000 Oe for **1** and **2**, respectively. The ac susceptibilities measured under these fields (Fig. S8) corroborates the decrease of the QTM contribution, while the corresponding Cole-Cole plots (Fig. S9, Tables S7-S8) unambiguously confirm the occurrence of a second relaxation process for **2**. These Cole-Cole plots were therefore fitted with a generalized Debye model and with a sum of two modified Debye functions[38] for **1** and **2**, respectively. Noticeably, a strong decrease in the α parameter values for **1** (< 0.05) is observed, indicating that the magnetic field causes a dramatic effect on the distribution of the relaxation times. Thus, a pertinent fitting of the temperature dependence of the relaxation time could be achieved for **1** and **3** using *CC-FIT2* and by considering solely a Raman process, $\tau^{-1} = CT^n$ (Table 2, Fig. 6 and S10), taken into account that the direct process should be inoperative for such weak values of the magnetic field. Remarkably, the obtained parameters are comparable with those obtained in zero dc fields (Table 2), but the associated small uncertainties indicate that, this in-field analysis for **1** and **3** could be considered as quantitative. Nevertheless, it was not possible to obtain a relevant fit with realistic parameters for **2**, which could be ascribed to the presence of two relaxations.

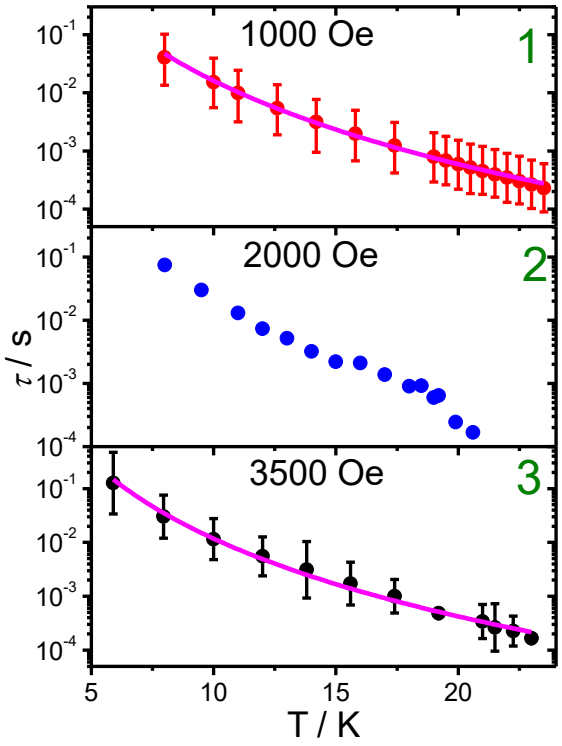

Fig. 6. Temperature dependence of the relaxation time for **1**-**3** using the ac susceptibility data in the presence of a dc field. The solid lines represent the fit with a Raman process.

Hence, the comparison between **1** and **3** for the in-field data clearly shows almost identical (within the standard deviation) *n* and *C* parameters. These parameters are however found slightly altered without considering the distribution of relaxation times (Table S5). Nevertheless the superposition on the τ vs. *T* plot for all compounds shows that they obviously follow the same trend (Fig. S10).

Magneto-structural correlations

At the exception of the large distribution of relaxation times for **2**, the magnetic analysis indicates therefore a comparable behaviour of the slow relaxation of the magnetization in **1**-**3** despite the slightly different structures. To get further insights, the orientation of the anisotropic axes of the ground Kramers doublets was evaluated by using the MAGELLAN software.[41] A negative charge on each nitrogen atom of the DAD ligand was considered. For **1**, the anisotropic axis does not pass through the center of the two DAD^{2H} ligands but is almost collinear (deviation of 16 and 18°) to the N2-Dy-N4 string (Fig. S11). The distance Dy-N2 is the second shortest one and is equal to 2.248(2) Å, while the Dy-N4 is longer 2.268(2) Å. However, the N2-Dy-N4 angle of 152.85° is closer to the linearity than any other N-Dy-N angles ranging from 109–119°. This may explain the deviation of the anisotropic axis with respect to the barycenter of the DAD^{2H} ligand. Moreover, the electrostatic influence of the K^+ ion most likely impacts the orientation of the anisotropic axis. In comparison, the anisotropic axis in complex **3** obtained with the same ligand, but with an uncoordinated Li^+ ion, passes through the middle of each DAD ligand (Fig. S11). This could be rationalized by the fact that the complex **3** is rather symmetrical regarding the two DAD^{2H} ligands and the N-Dy-N angles strongly deviate from linearity (ranging from 120 and 139°).[27] Consequently, it appears that the K^+/arene interaction results in the alteration of the DAD ligands repartition in the coordination sphere of the Dy^{3+} ion. Similarly than for **3**, the N1-Dy-N4 and N2-Dy-N3 angles in **2** are comparable and equal to 126 and 129°. In that case, the anisotropic axis is found to pass roughly through the barycentre of each DAD^{2Me} ligands (Fig. S11) which could be explained by a lesser electrostatic influence of the K^+ ion caused by a greater Dy^{3+}-K+ distance.

It appears that in these homoleptic complexes, the magnetic relaxation is dominated by the Raman process, which clearly shortcut the Orbach relaxation, despite a noticeable crystal-field splitting.[27] Determining the influence of the Raman relaxation is relatively complex since this process is known to depend on numerous parameters, such as the crystal density, the speed of sound in the solid and the strength of spin-phonon interactions.[42] Recently, the decisive role of vibrational modes on the Raman parameters has been evidenced.[9, 20, 22-23, 25, 43] **1** and **2** differ only by the nature of the substituent on the DAD ligand (H *vs.* Me). In contrast, **1** and **3** are based on the same ligand, but diverge by the nature of the counter-ion and its coordination mode. Hence, the comparable behaviours observed in our series suggest that: *i*) the K^+/arene interactions appear to unsuccessfully rigidify the structure and therefore does not shortcut the Raman relaxation; *ii*) introduction of methyl substituents on the DAD ligands does not alter specifically also the Raman relaxation. Consequently, this implies that, in this series based on the DAD ligands, the Raman process seems to be mainly controlled by vibrational modes in the close vicinity of the Dy^{3+} ion and most likely involves metal-ligand modes.

Analyzing the exact effect of the K^+-arene interactions over the slow relaxation is however far to be unequivocal due to very subtle structural effects and the predominance of the Raman relaxation. Yet, the possibility to alter the coordination sphere of the Dy^{3+} ion and in turn the orientation of the anisotropic axis through the electrostatic influence of the K^+ ion may provide new synthetic strategies to design high energy barriers SMMs involving a thermally activated relaxation.

Conclusions

In summary, we have reported here two new homoleptic Dy^{3+} complexes based on DAD ligands bearing different substitution groups and involving K^+/arene interactions. Both compounds exhibit a zero-field slow relaxation of the magnetization arising from a SMM behaviour. Although they differ by the nature of the substituent (H *vs.* Me) on the DAD ligands, both compounds exhibit comparable slow relaxation of the magnetization dynamics despite the observed changes in the Dy-N distances and the N-Dy-N sequence. In addition to the role of the substituent, the presence of K^+/arene interactions provides also a route to tune the coordination environment of the Dy^{3+} ion. Detailed magnetic analysis indicates that, in this series, the magnetic relaxation is governed by a Raman process, which only depends on molecular vibrations in the

close vicinity of the Dy^{3+} ion. This confirms that the in-depth understanding of the parameters affecting the Raman relaxation would be the key to improve the SMM features and achieve a high-temperature magnetic bistability.

Conflicts of Interest

There are no conflicts to declare.

Acknowledgements

The financial support of the Russian Science Foundation is highly acknowledged (Project № 17-73-30036). The X-ray study of **2** has been carried out in the framework of the Russian state assignment using the equipment of The Analytical Center of IOMC RAS. The French authors thank the University of Montpellier, CNRS and PAC of ICGM.

Notes and references

1 J. Luzon and R. Sessoli, *Dalton Trans.*, 2012, **41**, 13556-13567.
2 D. N. Woodruff, R. E. P. Winpenny and R. A. Layfield, *Chem. Rev.*, 2013, **113**, 5110-5148.
3 F. Troiani and M. Affronte, *Chem. Soc. Rev.*, 2011, **40**, 3119-3129.
4 L. Bogani and W. Wernsdorfer, *Nat. Mater.*, 2008, **7**, 179-186.
5 L. Ungur and L. F. Chibotaru, *Inorg. Chem.*, 2016, **55**, 10043-10056.
6 J.-L. Liu, Y.-C. Chen and M.-L. Tong, *Chem. Soc. Rev.*, 2018, **47**, 2431-2453.
7 J. Tang and P. Zhang, in *Lanthanide Single Molecule Magnets*, Springer Berlin Heidelberg, Berlin, Heidelberg, 2015, DOI: 10.1007/978-3-662-46999-6_2, pp. 41-90.
8 R. A. Layfield and M. Murugesu, *Lanthanides and Actinides in Molecular Magnetism*, Wiley, 2015.
9 M. J. Giansiracusa, A. K. Kostopoulos, D. Collison, R. E. P. Winpenny and N. F. Chilton, *Chem. Commun.*, 2019, **55**, 7025-7028.
10 N. F. Chilton, *Inorg. Chem.*, 2015, **54**, 2097-2099.
11 J. Liu, Y.-C. Chen, J.-L. Liu, V. Vieru, L. Ungur, J.-H. Jia, L. F. Chibotaru, Y. Lan, W. Wernsdorfer, S. Gao, X.-M. Chen and M.-L. Tong, *J. Am. Chem. Soc.*, 2016, **138**, 5441-5450.
12 S. K. Gupta, T. Rajeshkumar, G. Rajaraman and R. Murugavel, *Chem. Sci.*, 2016, **7**, 5181-5191.
13 M. Gregson, N. F. Chilton, A.-M. Ariciu, F. Tuna, I. F. Crowe, W. Lewis, A. J. Blake, D. Collison, E. J. L. McInnes, R. E. P. Winpenny and S. T. Liddle, *Chem. Sci.*, 2016, **7**, 155-165.
14 Y.-C. Chen, J.-L. Liu, L. Ungur, J. Liu, Q.-W. Li, L.-F. Wang, Z.-P. Ni, L. F. Chibotaru, X.-M. Chen and M.-L. Tong, *J. Am. Chem. Soc.*, 2016, **138**, 2829-2837.
15 Y.-S. Ding, N. F. Chilton, R. E. P. Winpenny and Y.-Z. Zheng, *Angew. Chem. Int. Edit.*, 2016, **55**, 16071-16074.
16 Y.-S. Meng, L. Xu, J. Xiong, Q. Yuan, T. Liu, B.-W. Wang and S. Gao, *Angew. Chem. Int. Edit.*, 2018, **57**, 4673-4676.
17 A. B. Canaj, S. Dey, E. R. Martí, C. Wilson, G. Rajaraman and M. Murrie, *Angew. Chem. Int. Edit.*, 2019, **58**, 14146-14151.
18 Y.-Z. Zheng, Y.-S. Ding, T. Han, Y.-Q. Zhai, D. Reta, N. F. Chilton and R. E. P. Winpenny, *Chem. Eur. J.*, 2020, **n/a**.
19 F. S. Guo, B. M. Day, Y. C. Chen, M. L. Tong, A. Mansikkamaki and R. A. Layfield, *Angew. Chem. Int. Ed. Engl.*, 2017, **56**, 11445-11449.
20 C. A. P. Goodwin, F. Ortu, D. Reta, N. F. Chilton and D. P. Mills, *Nature*, 2017, **548**, 439-442.
21 F.-S. Guo, B. M. Day, Y.-C. Chen, M.-L. Tong, A. Mansikkamäki and R. A. Layfield, *Science*, 2018, **362**, 1400-1403.
22 A. Lunghi, F. Totti, R. Sessoli and S. Sanvito, *Nat. Comm.*, 2017, **8**, 14620.
23 L. Escalera-Moreno, J. J. Baldoví, A. Gaita-Ariño and E. Coronado, *Chem. Sci.*, 2018, **9**, 3265-3275.
24 F.-S. Guo, B. M. Day, Y.-C. Chen, M.-L. Tong, A. Mansikkamäki and R. A. Layfield, *Angew. Chem. Int. Edit.*, 2017, **56**, 11445-11449.
25 A. Chiesa, F. Cugini, R. Hussain, E. Macaluso, G. Allodi, E. Garlatti, M. Giansiracusa, C. A. P. Goodwin, F. Ortu, D. Reta, J. M. Skelton, T. Guidi, P. Santini, M. Solzi, R. De Renzi, D. P. Mills, N. F. Chilton and S. Carretta, *Phys. Rev. B*, 2020, **101**, 174402.
26 A. A. Trifonov, B. Shestakov, J. Long, K. Lyssenko, Y. Guari and J. Larionova, *Inorg. Chem.*, 2015, **54**, 7667-7669.
27 J. Long, B. G. Shestakov, D. Liu, L. Chibotaru, Y. Guari, A. Cherkasov, G. K. Fukin, A. Trifonov and J. Larionova, *Chem. Commun.*, 2017, **53**, 4706-4709.
28 J. Long, A. O. Tolpygin, A. V. Cherkasov, K. A. Lyssenko, Y. Guari, J. Larionova and A. A. Trifonov, *Organometallics*, 2019, **38**, 748-752.
29 M. D. Taylor and C. P. Carter, *Journal of Inorganic and Nuclear Chemistry*, 1962, **24**, 387-391.
30 M. Svoboda and H. t. Dieck, *Journal of Organometallic Chemistry*, 1980, **191**, 321-328.
31 S. J. Lyle and M. M. Rahman, *Talanta*, 1963, **10**, 1177-1182.
32 Bruker, *APEX 3 and SAINT*, 2016, B. A. Inc., Madison, Winsconsin, USA.
33 P. CrysAlis, *Agilent Technologies: Wrocław, Poland*, 2014.
34 G. M. Sheldrick, *Acta Crystallogr., Sect. C: Struct. Chem.*, 2015, **71**, 3-8.
35 L. Krause, R. Herbst-Irmer, G. M. Sheldrick and D. Stalke, *J. Appl. Crystallogr.*, 2015, **48**, 3-10.
36 S. Kaufmann, M. Radius, E. Moos, F. Breher and P. W. Roesky, *Organometallics*, 2019, **38**, 1721-1732.
37 D. L. Clark, J. C. Gordon, J. C. Huffman, R. L. Vincent-Hollis, J. G. Watkin and B. D. Zwick, *Inorg. Chem.*, 1994, **33**, 5903-5911.
38 Y.-N. Guo, G.-F. Xu, Y. Guo and J. Tang, *Dalton Trans.*, 2011, **40**, 9953-9963.
39 D. Reta and N. F. Chilton, *Phys. Chem. Chem. Phys.*, 2019, **21**, 23567-23575.
40 K. R. Meihaus, S. G. Minasian, W. W. Lukens, S. A. Kozimor, D. K. Shuh, T. Tyliszczak and J. R. Long, *J. Am. Chem. Soc.*, 2014, **136**, 6056-6068.
41 N. F. Chilton, D. Collison, E. J. L. McInnes, R. E. P. Winpenny and A. Soncini, *Nat. Commun.*, 2013, **4**, 2551.
42 R. Orbach and B. Bleaney, *Proc. R. Soc. London A*, 1961, **264**, 458-484.
43 P. Evans, D. Reta, G. F. S. Whitehead, N. F. Chilton and D. P. Mills, *J. Am. Chem. Soc.*, 2019, **141**, 19935-19940.